AC Low-Frequency Characterization of Stopband Negative Group Delay Circuit

**Sofia Fenni[1], Fayrouz Haddad[1], Konstantin Gorshkov[2],
Bogdana Tishchuk[2], Antonio Jaomiary[3], Fabrice Marty[4], George Chan[5],
Mathieu Guerin[1, *], Wenceslas Rahajandraibe[1], and Blaise Ravelo[6]**

Abstract—This paper investigates the original circuit theory on stopband (SB) negative group delay (NGD) passive topology. The basic specifications of SB-NGD function are defined by considering the voltage transfer function (VTF) of the passive circuit. An original design method and experimentation tests of SB-NGD circuit are developed. The innovative theoretical analysis is elaborated from both magnitude and GD analytical expression of the VTF model from the resonant LC-series network passive topology. The mathematical existence condition of SB-NGD aspect is analytically explored in function of R, L, and C component parameters. The formulations of the basic equations enabling the calculation of the lumped components of the SB-NGD passive circuit in function of the desired specifications as NGD cut-off frequencies, NGD value and attenuation are established. To confirm the effectiveness of the original SB-NGD circuit theory, a proof-of-concept (POC) of SB-NGD circuit board is designed, simulated, fabricated, and experimented. As expected, despite the equivalent series resistor (ESR) effect of the inductor element, the theoretical modelling, simulation and measurement results are in good agreement. The SB-NGD behavior is confirmed with lower and upper cut-off frequencies, 0.7 kHz and 1.35 kHz, respectively. Furthermore, the corresponding NGD minimal values are $-33\,\mu s$ and $-11\,\mu s$, respectively.

1. INTRODUCTION

The first analytical investigation with pulse signal propagation enabling the illustration of the negative group delay (NGD) effect [1] was initially proposed in 1970s. But the counter intuitive effect related to the output signal advance compared to its input attracts the attention of certain researchers. Therefore, experimentations initially with optical systems were carried out by considering a pulse signal propagating through negative group velocity (NGV) media [2–5]. It was understood from the experimentation that certain media susceptible to operate with NGV behavior are capable to generate the NGD function.

After the first optical demonstration, the existence of the NGD effect becomes a research topic attracting some researchers in the area of electronic engineering [6–20]. Emphatically, the NGD effect was theoretically and experimentally investigated with R, L, and C elements, and operational amplifier based low-frequency (LF) circuits [6, 7]. It was pointed out from the electronic circuit-based study that the NGD effect is not in contradiction with the causality principle [6, 7]. Despite this LF circuit based NGD investigation, the question on the diversity of the circuit topologies capable to operate with NGD effect was opened. It was found that many circuits as the microwave structures designed with left-handed

[1] Aix-Marseille University, CNRS, University of Toulon, IM2NP UMR7334, Marseille, France. [2] ITMO University, Saint Petersburg, Russia. [3] Ecole Normale Supérieure pour l'Enseignement Technique (ENSET), BP O, Antsiranana 201, Madagascar. [4] Association Française de Science des Systèmes (AFSCET), Paris, France. [5] ASM Pacific Technology Ltd., Hong Kong, China. [6] Nanjing University of Information Science & Technology (NUIST), Nanjing, China.

negative refractive index (NRI) artificial transmission lines (TLs) [8, 9] can also generate the NGD effect. In parallel with the development of metamaterial-based microwave circuits, NGD experimentations in the gigahertz frequencies were also performed [8, 9]. However, the metamaterial periodical structure based NGD circuit operates in gigahertz frequencies with significant losses which can be more than 40 dB. Therefore, NGD researches [10–14] were conducted to design low-attenuation loss NGD circuits. As solution, different topologies of low-attenuation NGD circuits designed with distributed structures were proposed [10–14]. Many innovative challenges in different aspects were investigated. Some of distributed NGD circuits were designed under challenge in terms of compactness [13]. The tunability of NGD circuit was also investigated [14].

Despite the progress of tiny research activities on the NGD effect compared to that focus on the other electronic functions as filters, amplifiers, antennas, phase shifters, and attenuators, the NGD circuit design remains an open question to most of today electronic design engineers. A simple manner to study the NGD circuit becomes a fundamental function and an indispensable topic. In this way, the simplest approach to afford the NGD circuit design was initiated by considering the analogy between the filter and NGD functions [15, 16]. The concept of low-pass (LP) [15–18] and high-pass (HP) [15, 16, 19, 20] NGD circuits was innovatively introduced. Under this approach, we can classify the most developed topologies of microwave NGD circuits [6–14] as bandpass (BP) NGD-type circuit. Those developed BP-NGD type circuits were tentatively exploited for various applications notably in the areas of radio frequency(RF) and microwave engineering [21–24].

Nevertheless, so far, no investigation is available in the literature on the design of the innovative class of stop-band (SB) NGD topology. The main purpose of the present study is the development of an innovative circuit theory and also a design method of an SB-NGD passive topology. The proposed SB-NGD cell is constituted by a resonant LC-series network. We emphasize that different from the S-parameter based NGD investigation research work performed in [16], the present study is focused on the VTF modelling and also dedicated to low-frequency circuit analysis. The paper is organized in four successive sections as follows:

- Section 2 introduces the general configuration of an SB-NGD circuit. Based on the voltage transfer function (VTF) representation, the basic frequency domain function enabling the specification of the SB-NGD parameters will be defined.
- Section 3 is focused on the topological investigation of the resonant LC-series network-based passive topology. An innovative circuit theory including the SB-NGD analysis of LC-series network-based topology will be elaborated. Then, the synthesis formulas enabling the determination of values of the components in function SB-NGD function specifications will be established.
- Section 4 is the validation of the proposed SB-NGD circuit theory. A proof-of-concept (POC) of SB-NGD passive circuit operating in low-frequency (LF) will be described. Then, as validations, the SB-NGD NGD responses will be discussed by the comparison of calculations and simulations.
- Section 5 is the final conclusion.

2. DEFINITION OF STOP-BAND (SB) NGD SPECIFICATIONS

The present section describes the basic configuration of an SB-NGD circuit. The main parameters enabling the specifications of the SB-NGD circuit will be presented. The basic frequency domain responses necessary to specify an unfamiliar SB-NGD function will be defined.

2.1. General Configuration of SB-NGD Circuit Representation

Under analog manner as the classical circuits, the SB-NGD circuit theory can be elaborated from the equivalent voltage transfer function (VTF) exploration. To do this, the introduced passive topology can be theoretically assumed as a two-port circuit with input and output accesses, V_{in} and V_{out}, respectively, as represented by the general block diagram shown by Fig. 1.

For this SB-NGD circuit analysis, it seems more practical to consider the frequency responses. The analysis will be based on the VTF expressed by the following equation:

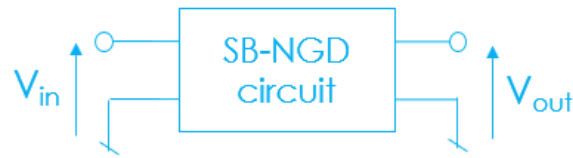$$N(s) = \frac{V_{out}(s)}{V_{in}(s)} \tag{1}$$

Figure 1. Two-port circuit diagram.

by taking the Laplace variable in function of angular frequency variable, $s = j\omega$.

2.2. Basic Analytical Definition

The main analytical parameters necessary for the SB-NGD circuit analysis are extracted from the transmittance by means of the magnitude, phase, and essentially the GD. These parametric quantities are theoretically denoted by:

   - The magnitude of the transmittance:

$$N(\omega) = |N(j\omega)| \tag{2}$$

   - The associated phase angle:

$$\varphi(\omega) = \arg[N(j\omega)] \tag{3}$$

   - And then, the GD expression:

$$\mathrm{GD}(\omega) = -\frac{\partial\varphi(\omega)}{\partial\omega}. \tag{4}$$

Similar to the filter theory, the SB-NGD response is defined in function of the existence of frequency band where the GD previously expressed in Equation (4) becomes negative:

$$\mathrm{GD}(\omega) < 0. \tag{5}$$

However, the SB-NGD response can be graphically represented as described in the following paragraph.

2.3. SB-NGD Ideal Specifications

The frequency domain diagrams enable the deep investigation of unfamiliar NGD functions. Fig. 2(a) and Fig. 2(b) depict the typical GD and magnitude of SB-NGD ideal responses, respectively. For better understanding, the different specifications associated with this diagram will be described in the following paragraph.

According to the ideal diagram of Fig. 2(a), the SB-NGD analysis is fundamentally the determination of the specifications of the circuit as:

   - the NGD cut-off frequencies:

$$\begin{cases} \omega_1 = 2\pi f_1 \\ \omega_2 = 2\pi f_2 > \omega_1 \end{cases} \tag{6}$$

   - which are the roots of the equation:

$$\mathrm{GD}(\omega) = 0 \Rightarrow \begin{cases} \mathrm{GD}(\omega_1) = 0 \\ \mathrm{GD}(\omega_2) = 0 \end{cases} \tag{7}$$

   - the NGD center frequency:

$$\omega_0 = 2\pi f_0, \tag{8}$$

   - the NGD bandwidth:

$$\Delta\omega = 2\pi\Delta f = \omega_2 - \omega_1, \tag{9}$$

   - and the NGD value:

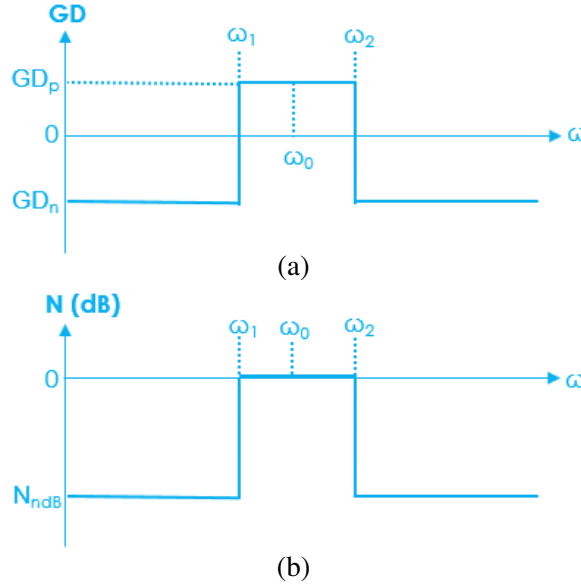$$\mathrm{GD}(\omega_0) = \mathrm{GD}_0 < 0. \tag{10}$$

(a)

(b)

Figure 2. (a) GD and (b) magnitude responses of ideal SB-NGD function.

In addition to the GD specifications, in the NGD frequency band or at the NGD center frequency, the magnitude given by Equation (2) can be defined in function of the given limit:

$$N(\omega_0) = A \leq 1 \tag{11}$$

Knowing these quantities, we can concretely perform the unfamiliar SB-NGD analysis applied to resonant RLC-network passive circuit in the following section.

3. THEORETICAL ANALYSIS OF THE RESONANT RLC-NETWORK BASED SB-NGD PASSIVE TOPOLOGY

The present section introduces the theoretical approach of the original SB-NGD passive topology. A two-port passive circuit constituted by a resonant RLC-network will be investigated. Then, the analysis and synthesis equations of the topology under study are formulated.

3.1. Frequency Responses of the Passive RLC-Network Circuit

The present SB-NGD theoretical analysis is focused on the LC-series lumped network-based topology introduced by Fig. 3. It acts as a two-port L-shape passive topology constituted by an LC-series network in parallel with a resistor R ended by a shunt resistor R_m. The access ports are referenced by input and output voltages, V_{in} and V_{out}. After the connection of input voltage source, V_{in}, the circuit operates with input current I_0.
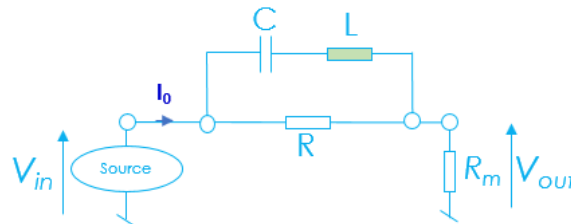

Figure 3. Topology of SB-NGD lumped circuit.

By means of voltage divider principle, the VTF introduced in Equation (1) can be written as follows:

$$N(s) = \frac{R_m}{R_m + Z(s)} \tag{12}$$

with the equivalent series impedance:

$$Z(s) = \frac{R(1 + LCs^2)}{1 + RCs + LCs^2}. \tag{13}$$

The associated transmittance can be expressed as:

$$N(j\omega) = \frac{1 - \dfrac{\omega^2}{\omega_0^2} + j\xi\dfrac{\omega}{\omega_0}}{\alpha\left(1 - \dfrac{\omega^2}{\omega_0^2}\right) + j\xi\dfrac{\omega}{\omega_0}} \tag{14}$$

with the resonance angular frequency:

$$\omega_0 = \frac{1}{\sqrt{LC}} \tag{15}$$

and the constant parameters:

$$\xi = R\sqrt{\frac{C}{L}} \tag{16}$$

$$\alpha = 1 + \frac{R_m}{R}. \tag{17}$$

Based on this VTF, the NGD circuit analysis will be elaborated in the following paragraph.

3.2. Magnitude and GD Expressions

The frequency domain magnitude (defined by Equation (2)) of the VTF given by Equation (14) is expressed as:

$$N(\omega) = \frac{\sqrt{\left(1 - \dfrac{\omega^2}{\omega_0^2}\right)^2 + \left(\xi\dfrac{\omega}{\omega_0}\right)^2}}{\sqrt{\alpha^2\left(1 - \dfrac{\omega^2}{\omega_0^2}\right)^2 + \left(\xi\dfrac{\omega}{\omega_0}\right)^2}}. \tag{18}$$

The associated phase response (defined by Equation (3)) can be written as:

$$\varphi(\omega) = \arctan\left[u(\omega)\right] - \arctan\left[\frac{u(\omega)}{\alpha}\right] \tag{19}$$

with:

$$u(\omega) = \frac{\xi\dfrac{\omega}{\omega_0}}{1 - \dfrac{\omega^2}{\omega_0^2}} = \frac{\xi\omega_0\omega}{\omega_0^2 - \omega^2} \tag{20}$$

Following the definition in Eq. (4), the derivative of this phase with respect to the angular frequency gives the GD expressed as:

$$\mathrm{GD}(\omega) = \frac{\partial u(\omega)}{\partial \omega}\left[\frac{1}{1 + u(\omega)^2} - \frac{\alpha}{\alpha^2 + u(\omega)^2}\right] \tag{21}$$

where:

$$\frac{\partial u(\omega)}{\partial \omega} = \frac{\dfrac{\xi}{\omega_0}\left[\left(1 - \dfrac{\omega^2}{\omega_0^2}\right)^2 + 2d\dfrac{\omega^2}{\omega_0^2}\right]}{\left(1 - \dfrac{\omega^2}{\omega_0^2}\right)^2}. \tag{22}$$

This GD expression will serve for the NGD analysis in the following subsection.

3.3. SB-NGD Theoretical Analysis

The present SB-NGD analysis is established from the previously elaborated magnitude and GD frequency responses.

3.3.1. Analysis at Particular Frequencies

The NGD analysis in the frequency domain can begin with the consideration of particular frequencies. Accordingly, at very low frequencies $\omega \approx 0$, we can simplify the RLC-network magnitude and GD as:

$$N(\omega \approx 0) = \frac{1}{\alpha} \tag{23}$$

$$GD(\omega \approx 0) = \frac{\xi(1 - \alpha)}{\alpha \omega_0}. \tag{24}$$

We can point out that this very low frequency GD is always negative for any values of circuit parameters, R_m, R, L, and C. Moreover, we can demonstrate that at the resonance, $\omega = \omega_0$, the frequency responses of our passive circuit become:

$$N(\omega_0) = 1 \tag{25}$$

$$\mathrm{GD}(\omega_0) = \frac{2(\alpha - 1)}{\xi \omega_0}. \tag{26}$$

From these analytical results, we can make a statement about the NGD function classification of the circuit under study. The necessary condition of SB-NGD function existence can be verified from these two equations in equation:

$$\begin{cases} \mathrm{GD}_n = \mathrm{GD}(\omega \approx 0) < 0 \\ \mathrm{GD}_n = \mathrm{GD}(\omega_0) > 0 \\ \mathrm{GD}(\omega > \omega_0) < 0 \end{cases} . \tag{27}$$

We can attentively verify from Equation (24):

$$1 - \alpha < 0 \Leftrightarrow 1 - 1 - \frac{R_m}{R} < 0. \tag{28}$$

This means that the necessary condition of SB-NGD behavior is analytically satisfied.

3.3.2. SB-NGD Existence Condition

The aim of the analysis at this stage is to verify the GD response graphically as shown in Fig. 2(a). By taking the normalized angular frequency:

$$x = \frac{\omega}{\omega_0} \tag{29}$$

we have:

$$\mathrm{GD}(x) = \frac{\dfrac{\xi(1 - \alpha)}{\omega_0}(1 + x^2)\left[\alpha x^4 - (\xi^2 + 2\alpha^2)x^2 + \alpha\right]}{\left[x^4 + (\xi^2 + 2)x^2 + 1\right]\left[\alpha^2 x^4 + (\xi^2 - 2\alpha^2)x^2 + \alpha^2\right]}. \tag{30}$$

In this case, Equation (7) is equivalent to:

$$\alpha x^4 - (\xi^2 + 2\alpha^2)x^2 + \alpha = 0 \tag{31}$$

It yields the discriminant given by:

$$\Delta_x = \xi^2(\xi^2 + 4\alpha). \tag{32}$$

It is noteworthy that this discriminant is always positive ($\Delta_x > 0$), for any value of the circuit parameters R_m, R, L, and C. Therefore, the associated roots which represent the cut-off frequencies of the NGD function can be expressed as follows:

$$\omega_1 = \frac{\omega_0 \sqrt{(\xi^2 + 2\alpha^2) - \xi\sqrt{\xi^2 + 4\alpha}}}{\sqrt{2\alpha}} \tag{33}$$

$$\omega_2 = \frac{\omega_0 \sqrt{(\xi^2 + 2\alpha^2) + \xi\sqrt{\xi^2 + 4\alpha}}}{\sqrt{2\alpha}}. \tag{34}$$

We can remark that:

$$\omega_1 \omega_2 = \omega_0^2. \tag{35}$$

In a nutshell, knowing that $1 - \alpha < 0$, according to the 2$^{\text{nd}}$ order polynomial mathematical theory, we can summarize the sign of the GD as addressed in Table 1.

Table 1. NGD behavior in function of the frequency bands.

Frequency band	Sign[GD(ω)]	Behavior of the RLC-circuit
$\omega < \omega_1$	sign[GD(ω)] = sign$(1 - \alpha) < 0$	NGD
$\omega_1 \leq \omega \leq \omega_2$	sign[GD(ω)] = sign$[-(1 - \alpha)] \geq 0$	Positive GD
$\omega \geq \omega_2$	sign[GD(ω)] = sign$(1 - \alpha) < 0$	NGD

As explored in the following subsection, the synthesis equation of the SB-NGD circuit can be extracted knowing the cut-off frequencies and GD values.

3.4. SB-NGD Design Equation

The synthesis design equations are aimed to determine the circuit parameters R, L, and C in function of the targeted SB-NGD specifications. In the present study, we can for example establish the design of the SB-NGD circuit in function of the desired:

- Center frequency, $\omega_0 = 2\pi f_0$,
- GD value, $\text{GD}_p < 0$, which should be linked to that attenuation at very LF ($\omega \approx 0$),
- And NGD bandwidth or cut-off frequencies.

By inverting the equation of the GD:

$$\text{GD}(\omega \approx 0) = \text{GD}_p, \tag{36}$$

proposed in Equation (28), we can determine

$$\xi = \frac{\alpha \omega_0 \text{GD}_p}{1 - \alpha}. \tag{37}$$

Substituting the last quantity into Equation (31), we can determine the attenuation as the root of the following one:

$$\alpha \omega_1^4 (1 - \alpha)^2 - \omega_0^2 \omega_1^2 \left(\alpha^2 \omega_0^2 \text{GD}_p^2 + 2\alpha^2 (1 - \alpha)^2\right) + \alpha(1 - \alpha)^2 \omega_0^4 = 0. \tag{38}$$

In this case, the upper cut-off frequency should be:

$$\omega_2 = \frac{\omega_0^2}{\omega_1}. \tag{39}$$

By inverting Equation (17), the value of resistor R can be obtained by taking R_m as a known parameter:

$$R = \frac{R_m}{\alpha - 1}. \tag{40}$$

From the resonance frequency equation given in Equation (15), we have:

$$C = \frac{1}{L\omega_0^2}. \tag{41}$$

Transitively, the coefficient given by Equation (16) becomes:

$$\xi = \frac{R}{L\omega_0^2}. \tag{42}$$

Therefore, we can calculate the inductor value by the formula:

$$L = \frac{-R_m}{\alpha\omega_0^3 \mathrm{GD}_p}. \tag{43}$$

To verify the feasibility of the developed SB-NGD LF circuit theory, a validation study is examined in the following section.

4. EXPERIMENTAL INVESTIGATION OF SB-NGD LF CIRCUIT

This section presents the experimental verification of the previously established SB-NGD circuit theory. A prototype of passive lumped circuit was designed, simulated, fabricated, and tested. The validation is based on the comparison between the calculated, simulated, and measured VTF results.

4.1. Experimental Setup Description

The relevance of the previously established theory was verified by designing, simulating, fabricating, and experimenting a POC of LFRLC-network based passive circuit. Fig. 4 displays the innovative illustrative diagram and experimentation of the SB-NGD circuit prototype.

The main purpose of the SB-NGD circuit experimentation is to practically measure the VTF in order to be compared with the analytical calculation from Equation (14). The challenging LF SB-NGD circuit which has never been done before is based on the use of sine signal generator which serves to sweep the frequency and an oscilloscope for simultaneously measuring the amplitudes and phases of both the input and output voltages. The SB-NGD circuit test was carried out with the equipment indicated by the specifications given in Table 2.

Table 2. Specifications of the SB-NGD test equipment's.

Description	References	Parameter	Value
Arbitrary function generator option	AKIP 4126/4A-X	Sampling rate	125 MS/s
		Bandwidth	25 MHz
Digital oscilloscope	AKIP 4122/3	Sampling rate	2 GS/s
		Bandwidth	100 MHz
Interconnection	Cable	BNC	1 m
	Connector	T-BNC	1 cm

With the fabricated SB-NGD circuit prototype, the formulation method of the NGD responses is indicated in the following subsection.
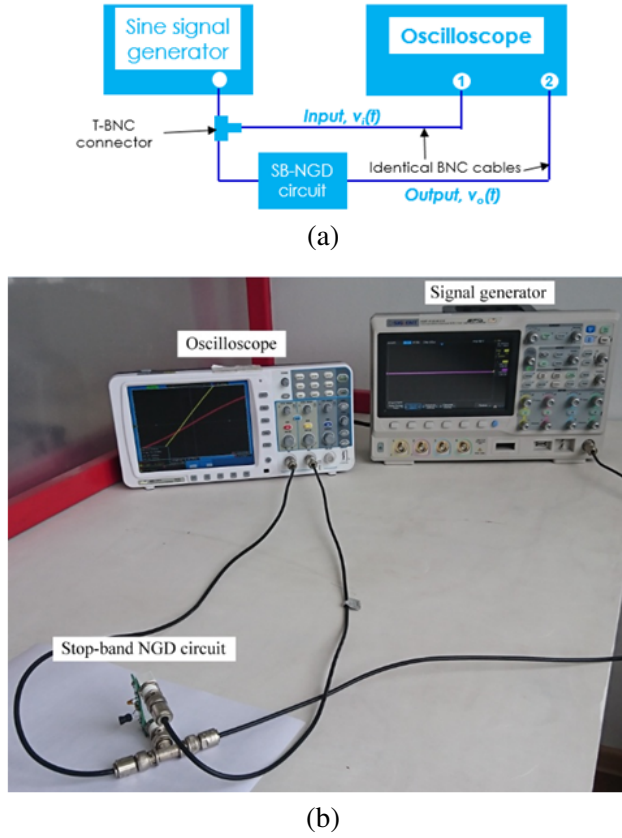
(a)

(b)

Figure 4. (a) Illustrative diagram and (b) photograph of the SB-NGD circuit prototype experimental setup.

4.2. Formulation of Measured SB-NGD Responses

The measured SB-NGD responses from the experimental setup introduced in the previous subsection are generated from the input and output sine wave voltages. The t-time dependent input sine signal can be expressed in function of the test frequency, f_k, and amplitude, $A_{\max}$, by the equation:

$$v_{in}(t) = A_{\max} \sin(2\pi f_k t). \tag{44}$$

Acting as a linear time-invariant, the associated output signal can be expressed by:

$$v_{out}(t) = B_{\max} \sin(2\pi f_k t + \Delta\varphi). \tag{45}$$

The HP-NGD circuit measurement consists originally in sweeping the frequency f_k of the input sine signal from $f_{\min} = 300\,\text{Hz}$ to $f_{\max} = 3.7\,\text{kHz}$. During the test, we choose the frequency step equal to $\Delta f = 50\,\text{Hz}$. The input signal was limited by the time width of $\Delta t = 40\,\mu\text{s}$. We recorded during the tests the amplitudes and phases of the input and output sine signals. Then, the measured amplitudes and phase shift of the measured circuit VTF were calculated from the classical equations:

$$T_{\text{measured}}(f_k) = \frac{B_{\max}(f_k)}{A_{\max}(f_k)} \tag{46}$$

$$\varphi_{\text{measured}}(f_k) = \Delta\varphi(f_k). \tag{47}$$

Accordingly, the GD response is determined by:

$$\text{GD}_{\text{measured}}(f_k) = \frac{\varphi_{\text{measured}}(f_k) - \varphi_{\text{measured}}(f_{k-1})}{2\pi(f_k - f_{k-1})} \tag{48}$$

where the integer k varies from 2 to $k_{\max}$. $A_{\max}$ and $B_{\max}$ are the input and output signal amplitudes:

$$k_{\max} = Ent \left[\frac{f_{\max} - f_{\min}}{\Delta f} \right]. \tag{49}$$

In this equation, the quantity, $Ent[x]$, presents the superior integer part of real x. By using the developed SB-NGD circuit measurement techniques, we obtained the results explored in the following section.

### 4.3. Description of the Designed and Fabricated SB-NGD Circuit POC

A POC of circuit board prototype was considered to verify the experimental validity of the SB-NGD function. The POC of the tested SB-NGD circuit was designed with ideal component values calculated from the synthesis equations of R, L, and C proposed in Sections 3–5. Discrete resistor, inductor, and capacitor lumped components commercially available were considered for the innovative SB-NGD function experimentation. Then, the circuit prototype was implemented with the nominal components available in our laboratory. The chosen component values are addressed by Table 3. The SB-NGD circuit POC was designed and simulated in the ADS® schematic environment of the electronic and RF/microwave design simulator from Keysight Technologies®. Fig. 5(a) depicts the schematic of the simulated SB-NGD circuit in the ADS® environment. The top view photograph of the fabricated circuit prototype board is shown in Fig. 5(b).

Table 3. SB-NGD circuit POC component values.

Description	Parameter	Nominal value
Resistor	R	$10\,\Omega$
	R_m	$10\,\Omega$
Inductor	L	$5.6\,\mathrm{mH}$
	R_l	$13.3\,\Omega$
Capacitor	C	$4.7\,\mu\mathrm{F}$

The components are soldered on an FR4-epoxy dielectric substrate with copper electrical interconnection traces. The two access ports of the circuit are represented by the BNC connectors.

The verification study consists in comparing the simulated and measured results from the circuit POC and prototype shown by Fig. 5 with the ideal model which represent the analytical calculated results from MATLAB® programming. The investigation on the validation study will be discussed in the next subsection.
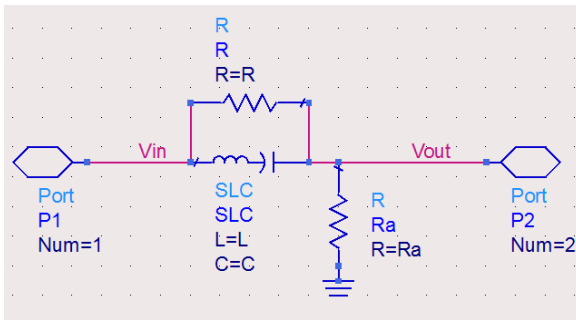
(a)

(b)

Figure 5. (a) Simulated schematic and (b) photograph of SB-NGD circuit prototype.

4.4. Discussion on the Validation Results

The present subsection investigates the comparative results from calculation, simulation, and measurement of the tested SB-NGD circuit. However, as we did not find an ideal inductor without parasitic effect, we considered a coilcraft by taking into account the equivalent series resistance (ESR). The influence of ESR on SB-NGD response will be discussed. Then, the final validation will be discussed.

4.4.1. Analysis of SB-NGD Response ESR Effect

In a real case, the coilcraft self-inductance component implemented on the prototype shown by Fig. 5(b) is significantly affected by parasitic effect. The present subsection is focused on the study of this parasitic effect by means of ESR. Fig. 6 depicts the SB-NGD circuit integrating the ESR element represented by the series resistor R_l.
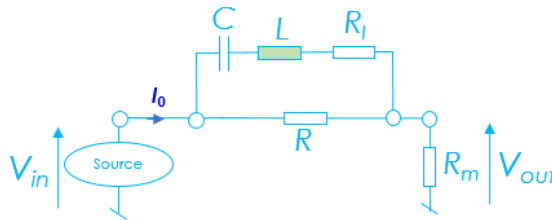

Figure 6. SB-NGD lumped circuit integrating parasitic ESR element of the self-inductor.

Because of this parasitic resistance one, the VTF of our POC circuit is modified as:

$$N_{\text{ESR}}(s) = \frac{R_m}{R_m + Z_{\text{ESR}}(s)} \tag{50}$$

with:

$$Z_{\text{ESR}}(s) = \frac{1}{\dfrac{1}{R} + \dfrac{Cs}{1 + LCs^2 + R_lCs}} = \frac{R(1 + R_lCs + LCs^2)}{1 + (R + R_l)Cs + LCs^2}. \tag{51}$$

The comparisons between the SB-NGD circuits with and without ESR were investigated based on ADS® simulation and calculated model. The obtained frequency domain results are displayed by Fig. 7. The ideal circuit simulated (presented by "Simu.", plotted in dotted red curve) and calculated (noticed by "Calc.", plotted in solid black curve) VTF magnitudes, phases, and GDs are plotted in Fig. 7(a), Fig. 7(b), and Fig. 7(c), respectively. Hence, the ESR including circuit results are simultaneously plotted in dotted blue-sky curves and solid navy-blue curves of Fig. 7(a), Fig. 7(b), and Fig. 7(c), respectively. First of all, a very good agreement between the simulated and calculated results is confirmed for the three frequency responses. In addition, despite the ESR effect, the SB-NGD behavior is still conserved as illustrated by the GD responses of Fig. 7(c). The main frequency characteristics (NGD central frequency, f_0, NGD lower optimal frequency, f_a, and NGD upper optimal frequency, f_b) of the SB-NGD circuit POC are indicated by Fig. 8. Nevertheless, significant differences between the optimal frequencies of maximal magnitude and GD values are listed in Table 4.

4.4.2. Experimental Validation of SB-NGD Magnitude and Phase Responses

In a more obvious representation, the model ("solid black curve"), simulation ("dotted red curve"), and measurement ("dashed blue curve") results of VTF magnitude and phase are displayed by Fig. 9(a) and Fig. 9(b), respectively. As expected, for both cases of frequency responses, a good fitting is observed over the entire considered frequency range. These results confirm the effectiveness of the theoretical modelling for predicting the responses of the SB-NGD topology.
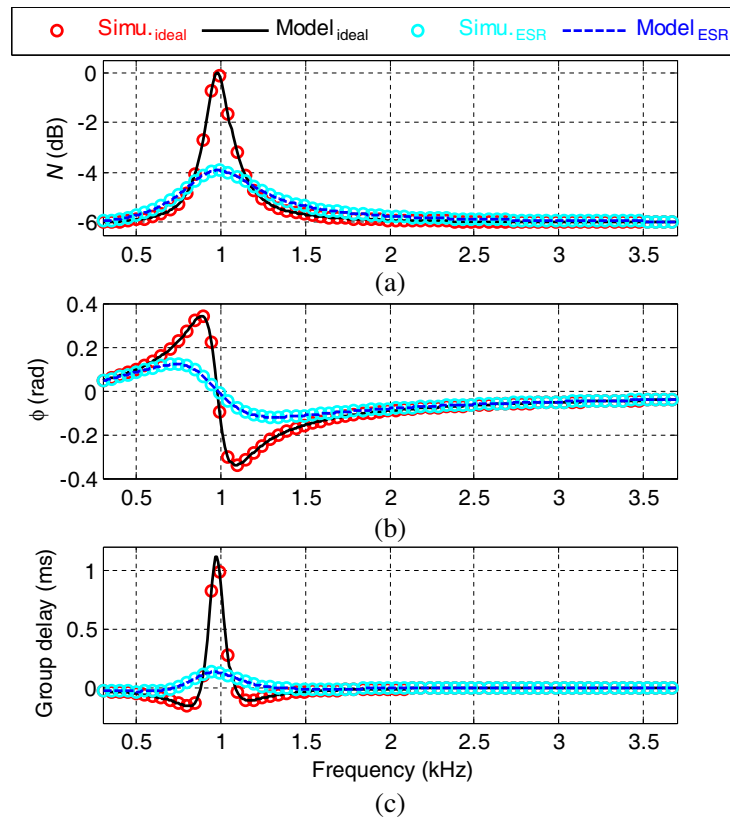
Figure 7. Comparisons of (a) magnitude, (b) phase, and (c) GD responses of the SB-NGD circuit POC with and without ESR.
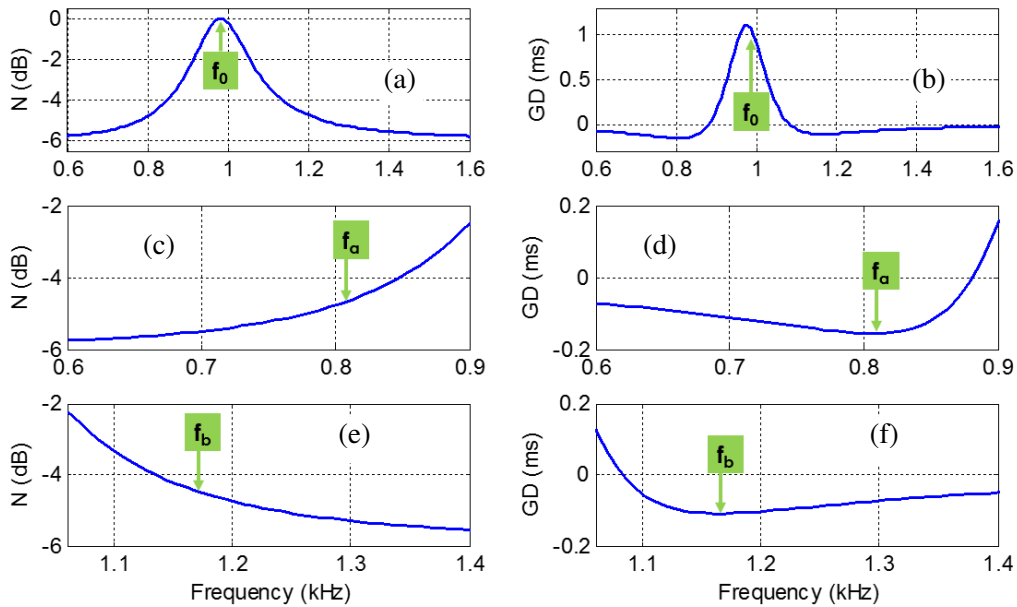

Figure 8. Magnitude ((a) wide, (b) lower, and (c) upper frequency bands) and GD ((a) wide, (b) lower, and (c) upper frequency bands) responses of the SB-NGD circuit POC with ESR.
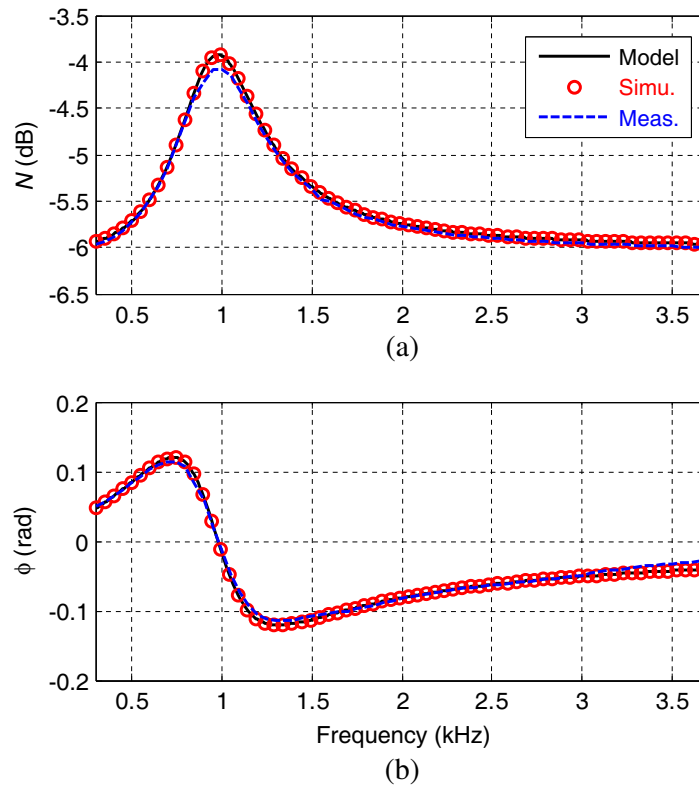
Figure 9. Magnitudes and phases of the SB-NGD circuit prototype shown in Fig. 5.

Table 4. Optimal frequencies of maximal magnitude of the calculated, simulated and measured results from ideal, parasitic and measured cases.

| Considered parameters	Type of circuit	Configuration	Frequency (Hz)	Magnitude (dB)	GD (µs)
Maximal gain at central frequency, f_0	Ideal	Simulation	994.89	−0.12	0.99
		Model	978.35	0.00	1.12
	ESR	Simulation	994.89	−3.93	127.52
		Model	978.35	−3.92	131.10
		Measurement	950.00	−4.08	108.72
Optimal lower frequency, f_a	Ideal	Simulation	796.35	−4.82	−0.16
		Model	804.62	−4.72	−0.16
	ESR	Simulation	498.54	−5.72	−32.57
		Model	515.09	0.52	−32.61
		Measurement	550.00	−5.62	−33.06
Optimal upper frequency, f_b	Ideal	Simulation	1193.43	−4.70	−0.11
		Model	1168.61	−4.45	−0.11
	ESR	Simulation	1640.15	−5.52	−11.17
		Model	1582.24	0.53	−11.19
		Measurement	2000.00	−5.77	−11.72
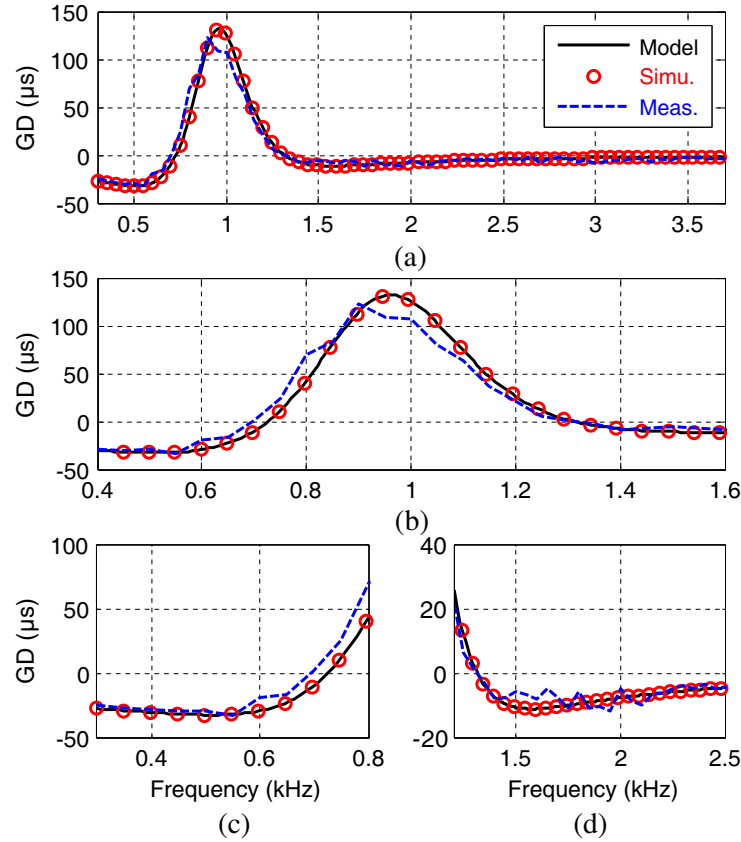
Figure 10. GDs of the SB-NGD circuit prototype shown in Fig. 5.

Table 5. NGD cut-off frequencies and the corresponding attenuation.

Type of circuit	Configuration	f_1 (Hz)	f_1 (Hz)	$N(f_1)$ (dB)	$N(f_2)$ (dB)
Ideal	Simulation	300.00	1789.05	−5.99	−5.86
	Model	879.08	3700.00	−3.21	−6.00
ESR	Simulation	730.17	1317.52	−4.97	−4.97
	Model	746.72	1342.34	−4.89	−5.04
	Measurement	700.00	1350.00	−5.15	−5.09

4.4.3. Experimental Validation of SB-NGD GD Response

The modelled, simulated, and experimented GDs of the tested circuit shown by Fig. 5 are displayed by Fig. 10. We recall that the model is from the analytical expression of VTF given by Equation (51). We can distinguish the three different frequency bands in the wide band plots of Fig. 10(a) and Fig. 10(b). Then, the lower and upper NGD cut-off frequencies are observed in Fig. 10(c) and Fig. 10(d). The lower and upper cut-off frequencies and the associated attenuations are indicated by Table 5. It can be seen clearly from the three configurations of validation study that the simulated and tested circuit behaves as a SB-NGD function.

All the obtained results of the present section concretely confirm the feasibility of the SB-NGD function generation with the resonant RLC-network based lumped circuit. The most important remark from this study is that the first-time investigation on how to design a SB-NGD passive circuit is experimentally validated with innovative LF test technique.

5. CONCLUSION

A particularly original circuit theory on a resonant LC-network based innovative SB-NGD passive topology is developed. The main specifications of the unfamiliar SB-NGD function are defined by inspiration from the filter circuit theory. By means of the classical frequency responses, the main parameters of SB-NGD function are analytically introduced.

The SB-NGD behavior analytical approach is elaborated from the VTF of two-port passive topology. First, a canonical form of VTF is established in function of the R, L, and C components constituting the considered topology. The GD values and frequency parameters are expressed. The existence condition of the SB-NGD aspect is also analytically demonstrated. Then, the synthesis equations determining each parameter are formulated in function of the SB-NGD specifications defined during the design phase.

The validity of the original SB-NGD circuit theory is verified by the comparison between theoretical, simulated, and experimental investigations. A POC constituted by discrete lumped components was designed and considered to fabricate an SB-NGD circuit prototype. As expected, the calculated, simulated, and measured results confirm the feasibility of the SB-NGD behavior with resonant LC-network circuit prototype.

In the continuation of the study, some parametric studies illustrating the robustness of the SB-NGD circuit will be investigated. In addition to the RF and microwave application proposed in [21–23], ongoing research work is currently in progress notably on potential applications of SB-NGD circuits in the electrical and electronic system as introduced in:

- To reduce the cable delay [25], we are developing an equalization technique as introduced in [24, 26] and
- The distorted signal reconstruction proposed in [27].

REFERENCES

1. Garrett, C. G. B. and D. E. McGumber, "Propagation of a Gaussian light pulse through an anomalous dispersion medium," *Phys. Rev. A*, Vol. 1, 305–313, 1970.
2. Chu, S. and S. Wong, "Linear pulse propagation in an absorbing medium," *Phys. Rev. Lett.*, Vol. 48, 738–741, 1982.
3. Ségard, B. and B. Macke, "Observation of negative velocity pulse propagation," *Phys. Lett. A*, Vol. 109, 213–216, 1985.
4. Macke, B. and B. Ségard, "Propagation of light-pulses at a negative group-velocity," *Eur. Phys. J. D*, Vol. 23, 125, 2003.
5. Munday, J. N. and W. M. Robertson, "Observation of negative group delays within a coaxial photonic crystal using an impulse response method," *Optics Communications*, Vol. 273, No. 1, 32–36, 2007.
6. Mitchell, M. W. and R. Y. Chiao, "Negative group delay and "fronts" in a causal system: An experiment with very low frequency bandpass amplifiers," *Phys. Lett. A*, Vol. 230, Nos. 3–4, 133–138, Jun. 1997.
7. Mitchell, M. W. and R. Y. Chiao, "Causality and negative group-delays in a simple bandpass amplifier," *Am. J. Phys.*, Vol. 66, 14–19, 1998.
8. Siddiqui, O. F., M. Mojahedi, and G. V. Eleftheriades, "Periodically loaded transmission line with effective negative refractive index and negative group velocity," *IEEE Trans. Antennas Propagat.*, Vol. 51, No. 10, 2619–2625, Oct. 2003.
9. Markley, L. and G. V. Eleftheriades, "Quad-band negative-refractive-index transmission-line unit cell with reduced group delay," *Electronics Letters*, Vol. 46, No. 17, 1206–1208, Aug. 2010.
10. Ahn, K.-P., R. Ishikawa, A. Saitou, and K. Honjo, "Synthesis for negative group delay circuits using distributed and second-order RC circuit configurations," *IEICE Trans. on Electronics*, Vol. E92-C, No. 9, 1176–1181, 2009.

11. Kandic, M. and G. E. Bridges, "Asymptotic limits of negative group delay in active resonator-based distributed circuits," *IEEE Transactions on Circuits and Systems I: Regular Papers*, Vol. 58, No. 8, 1727–1735, Aug. 2011.

12. Wu, C.-T. M. and T. Itoh, "Maximally flat negative group delay circuit: A microwave transversal filter approach," *IEEE Trans. Microw. Theory Techn.*, Vol. 62, No. 6, 1330–1342, Jun. 2014.

13. Liu, G. and J. Xu, "Compact transmission-type negative group delay circuit with low attenuation," *Electronics Letters*, Vol. 53, No. 7, 476–478, Mar. 2017.

14. Chaudhary, G. and Y. Jeong, "Tunable center frequency negative group delay filter using coupling matrix approach," *IEEE Microwave Wireless Component Letters*, Vol. 27, No. 1, 37–39, 2017.

15. Ravelo, B., "Similitude between the NGD function and filter gain behaviours," *Int. J. Circ. Theor. Appl.*, Vol. 42, No. 10, 1016–1032, Oct. 2014.

16. Ravelo, B., "On low-pass, high-pass, bandpass, and stop-band NGD RF passive circuits," *URSI Radio Science Bulletin*, Vol. 2017, No. 363, 10–27, Dec. 2017.

17. Ravelo, B., "First-order low-pass negative group delay passive topology," *Electronics Letters*, Vol. 52, No. 2, 124–126, Jan. 2016.

18. Wan, F., J. Wang, B. Ravelo, J. Ge, and B. Li, "Time-domain experimentation of NGD active RC-network cell," *IEEE Trans. Circuits and Systems II: Express Briefs*, Vol. 66, No. 4, 562–566, Apr. 2019.

19. Ravelo, B., "High-pass negative group delay RC-network impedance," *IEEE Trans. CAS II: Express Briefs*, Vol. 64, No. 9, 1052–1056, Sept. 2017.

20. Wan, F., X. Huang, K. Gorshkov, B. Tishchuk, X. Hu, G. Chan, F. E. Sahoa, S. Baccar, M. Guerin, W. Rahajandraibe and B. Ravelo, "High-pass NGD characterization of resistive-inductive network based low-frequency circuit," *COMPEL — The International Journal for Computation and Mathematics in Electrical and Electronic Engineering*, 1–19, 2021.

21. Choi, H., Y. Jeong, C. D. Kim, and J. S. Kenney, "Bandwidth enhancement of an analog feedback amplifier by employing a negative group delay circuit," *Progress In Electromagnetics Research*, Vol. 105, 253–272, 2010.

22. Zhu, M. and C.-T. M. Wu, "Reconfigurable series feed network for squint-free antenna beamforming using distributed amplifier-based negative group delay circuit," *Proc. 2019 49th European Microwave Conference (EuMC)*, 256–259, Paris, France, Oct. 1–3, 2019.

23. Mirzaei, H. and G. V. Eleftheriades, "Realizing non-Foster reactive elements using negative-group-delay networks," *IEEE Trans. Microw. Theory Techn.*, Vol. 61, No. 12, 4322–4332, Dec. 2013.

24. Ravelo, B., S. Lalléchère, A. Thakur, A. Saini, and P. Thakur, "Theory and circuit modelling of baseband and modulated signal delay compensations with low- and band-pass NGD effects," *Int. J. Electron. Commun. (AEÜ)*, Vol. 70, No. 9, 1122–1127, Ed. Elsevier, Sept. 2016.

25. Cholachue, C., B. Ravelo, A. Simoens, and A. Fathallah, "Fast S-parameter TAN model of N-port lumped structures," *IEEE Access*, Vol. 7, No. 1, 72505–72517, Dec. 2019.

26. Ravelo, B., F. Wan, W. Rahajandraibe, and N. M. Murad, "Cable delay cancellation with low-pass NGD function," *Proc. of 2020 International Symposium on Electromagnetic Compatibility — EMC EUROPE*, 1–5, Rome, Italy, Sept. 23–25, 2020.

27. Ravelo, B., W. Rahajandraibe, Y. Gan, F. Wan, N. M. Murad, and A. Douyère, "Reconstruction technique of distorted sensor signals with low-pass NGD function," *IEEE Access*, Vol. 8, No. 1, 92182–92195, Dec. 2020.